Towards understanding the robust strengthening of ENSO and extreme El Niño events with global warming in CMIP6

Ulla K. Heede (ulla.heede@yale.edu)
Yale University
Alexey V. Fedorov
Yale University

Research Article

Keywords: El Niño, ENSO, CMIP6, Climate Change, extreme events

Posted Date: June 17th, 2022

DOI: https://doi.org/10.21203/rs.3.rs-1731142/v1

Additional Declarations: No competing interests reported.

Version of Record: A version of this preprint was published at Climate Dynamics on June 25th, 2023. See the published version at https://doi.org/10.1007/s00382-023-06856-x.

Abstract

The El Niño Southern Oscillation (ENSO) has profound implications for weather patterns across the globe, and yet there is no consensus on its response to global warming. Several modelling studies suggest a stronger ENSO in global warming scenarios, while other studies find ENSO weakening. Using a broad range of models of the Coupled Model Intercomparison Project phase 6 (CMIP6) and four different types of warming experiments, here we show that the majority of the models predict a stronger ENSO by century-end in Shared Social Pathway (SSP) experiments, and in idealized 1pctCO_2 and abrupt 4xCO_2 experiments. Several models, however, predict no change or ENSO weakening, especially in the idealized experiments. For most models the strongest forcing (abrupt-4xCO_2) is not associated with the strongest ENSO response, while differences between the models are much greater than between warming scenarios. For the long-term (1000 years) response the models disagree even on the sign of change. Furthermore, changes in ENSO SST variability appear to be poorly correlated with the tropical mean state change, while changes in ENSO rainfall variability correlate well with changes in the mean state and, especially, ENSO SST variability. Evaluating changes in the Bjerknes Stability Index for a subset of models we find it to be a poor predictor for ENSO strengthening as this index typically suggests greater stability with warming. We hypothesize that changes to ENSO stability are offset by increases in atmospheric noise or/and potential nonlinear effects. Thus, a robust inter-model mechanism is still lacking to explain a stronger ENSO simulated with global warming, and caution should be exercised when considering ENSO changes based on a single model or warming scenario.

1. Introduction

The El Niño Southern Oscillation (ENSO) is the strongest interannual oscillation in Earth's climate, with dramatic impacts on weather patterns and extreme events in the tropics and beyond (Cai et al. 2021; McPhaden, Santoso, and Cai 2020). El Niño conditions are characterized by warm central and/or eastern Pacific sea surface temperature (SST) anomalies, reduced easterly trade winds and the corresponding slope of the ocean thermocline, and eastward shift of atmospheric convection. El Niño can lead to flooding in South America but drought and forest fires in areas bordering the western Pacific (Ropelewski and Halpert 1987). In addition, due to its effect on atmospheric planetary waves, ENSO affects a range of whether phenomena outside the tropical Pacific via teleconnections, and the signature of ENSO has been observed on all seven continents (Yeh et al. 2018).

Whether ENSO is already changing or will change with future warming, and, in particular, whether this change will lead to stronger and/or more frequent El Nino events is of great importance for timely implementation of societal adaptation and mitigation strategies. However, despite the importance of ENSO in Earth's climate, much uncertainty still remains concerning these questions.

It has long been known that ENSO depends on changes in the mean state tropical Pacific (Fedorov and Philander 2000, 2021; Fedorov et al. 2020; An and Jin 2020, Jin et al. 2006; DiNezio et al. 2012). There is broad consensus models participating in the Coupled Model Intercomparison Project, phase 6 (CMIP6) that the Walker cell will slow down with global warming, leading to enhanced warming of the eastern and central equatorial Pacific by century-end (e.g. Heede and Fedorov 2021). This enhanced warming of the eastern Pacific can be understood in terms of both atmospheric and oceanic mechanisms acting to reduce equatorial trade winds and eastern Pacific upwelling (U. K. Heede, Fedorov, and Burls 2020; 2021; Vecchi et al. 2006). Despite this consensus on future mean state warming in the equatorial Pacific, and the known links between mean state and ENSO characteristics, there is no robust consensus among climate models concerning the response of ENSO to global warming. A number of papers have suggested stronger ENSO in future climates in CMIP5 models, in particular based on precipitation metrics (Huang and Xie 2015; Cai et al. 2015), or based on metrics that isolate certain models (Cai et al. 2018). The tendency for ENSO to be stronger in future warming scenarios has also been reported for subsets of CMIP6 models (Fredriksen et al. 2020, 6; Cai et al. 2021; Brown et al. 2020). Cai et al. 2018 suggests two mechanisms that drive stronger eastern Pacific El Nino events: a stronger coupling between wind stress and SST in the eastern Pacific, and a stronger coupling between ocean feedbacks and wind stress due to enhanced upper ocean stratification.

Opposing Cai's et al. findings, several recent studies have argued that ENSO strength may decrease with warming (Christian Wengel et al. 2021; Callahan et al. 2021; Kohyama, Hartmann, and Battisti 2018). These studies typically rely on abrupt CO_2

quadrupling experiments and argue that increased thermodynamic damping and decreased ocean feedbacks among other mechanisms lead to a more stable ENSO with warming. Kohyama et al. (2018) in particular argues that enhanced ocean stratification leads to a stiffer thermocline and a decrease in ENSO non-linearity in contrast with the findings of Cai et al. (2018). These disagreements highlight that changes in different feedbacks due to changes in the mean state and ocean-atmosphere coupling can partially compensate each other leading to unanticipated results.

The goal of this study is to attempt to reconcile these divergent views of how ENSO responds to warming as well as provide more detailed insight into how ENSO changes within the CMIP6 models than previous studies have done (i.e. Fredriksen et al. 2020; Cai et al. 2022), using a broader range of models and climate scenarios. As one set of studies finding a stronger ENSO primarily rely on the 21st century SSP scenarios, while another set of studies finding a weaker ENSO uses the abrupt CO_2 quadrupling experiments, we provide an overview of how models respond across these idealized and realistic forcing experiments to elucidate any uncertainty associated with a given experiment-type.

Furthermore, we aim to explore how the various mechanisms proposed for a stronger or weaker ENSO may manifest across different models and document how ENSO changes might be linked to the tropical Pacific mean state. Finally, to explore whether the transient response differs from the long-term response in the abrupt-4xCO_2 experiments as proposed by Callahan et al. (2021), we include three 1000-year simulations. To our knowledge, no study has compared ENSO changes across a broad range of idealized and realistic forcing scenarios in CMIP6 models, as well as attempted to link those changes to tropical mean state changes in a comprehensive manner.

2. Methods

2.1 CMIP6 archive

We analyze two types of experiments from the Climate Model Intercomparison Project Phase 6 (CMIP6) archive. The first type consists of two hypothetical or idealized CO_2-only experiments: abrupt-4xCO_2 rise and 1pctCO_2 gradual CO_2 rise (1% per year) where CO_2-increases are relative to a pre-industrial level of 280 ppm. The second type has full-forcing experiments, including two future scenarios, SSP5-8.5 which is a high-emission scenario and SSP1-2.6, in which emissions peak and decline in the 21st century (O'Neill et al. 2016).

We use a total of 20 CMIP6 models in our overview analysis (see Table 1), utilizing surface temperature, column precipitation flux, and zonal wind stress. The criterion for including a given model into the analysis is whether it has surface temperature data available for at least three ensemble members for the SSP5-8.5 scenario. Some models do not have all datasets available for all experiments, and models are excluded whenever data is not available. For the idealized warming experiments (4xCO_2 and 1pctCO_2), where ensemble members are generally not available, we use a single ensemble member, and for the SSP scenarios we use the ensemble-mean results based on three members. We include 85, 150 and 200 years of simulation for the SSP experiments, the idealized experiments and the piControl experiment respectively.

Table 1

Overview of models used and their associated marker.

Model	Marker
ACCESS-CM2	
ACCESS-ESM1-5	
CanESM5-CanOE	
CanESM5	
CESM2-WACCM	
CESM2	
CNRM-CM6-1	
CNRM-ESM2-1	
EC-Earth3	
EC-Earth3-Veg	

Model	Marker
FGOALS-g3	
FIO-ESM-2-0	
HadGEM3-GC31-LL	
HadGEM3-GC31-MM	
IPSL-CM6A-LR	
KACE-1-0-G	
MIROC6	
MIROC-ES2L	
MPI-ESM1-2-LR	
UKESM1-0-LL	

2.2 Metrics

We define the amplitude of ENSO SST variability as the standard deviation of band-passed temperature anomalies in the frequency range between 1.5 to 7 years from which the climatology was subtracted for the central-east Pacific (180–280ºE). This region is chosen to capture ENSO changes across both the central and eastern Pacific following Ferrett and Collins (2019). We further define the mean state zonal Pacific gradient as the difference between time mean anomalies of the western Pacific (120^{o}-180^{o} E) and the central-eastern Pacific (180^{o} -280^{o} E). While the issue of Central Pacific (CP) versus Eastern Pacific (EP) El Niño events has been discussed as a potential culprit in using set boxes in other studies (Cai et al. 2018), we find that the estimated ENSO changes are not very sensitive to the chosen box, and that most models show a consistent change in standard deviation across both the central and eastern equatorial Pacific.

Similarly, we define the strength of ENSO rainfall variability as the standard deviation of band-passed precipitation anomalies in the frequency range between 1.5 to 7 years from which the climatology is subtracted for the central-east Pacific (180–280ºE). We define extreme El Niño events as events with warm temperature anomalies in the central-east Pacific (180–280ºE), exceeding 2 standard deviations. While 2.5 standard deviations are sometimes used to define an extreme event (Yu and Fedorov 2020), we chose 2 to get robust statistics as most models have few events of 2.5 standard deviation magnitude in timeframe of 85 to 200 years. All changes are computed relative to the piControl experiment. While some studies compare SSP scenarios to the historical period (i.e. Cai et al. 2022), we compare all experiment types to the piControl experiment in order to facilitate a fair comparison between idealized experiments and future warming scenarios. For the majority of models, the strength of ENSO in the piControl experiment is similar to the historical experiment.

2.3 Bjerknes Stability Index

To evaluate possible links between mean state changes and ENSO response to warming, we use the Bjerknes Stability Index (Jin, Kim, and Bejarano 2006). The Bjerknes Index (BJ index, in units of yr^{-1}) assumes that ENSO dynamics are controlled by the recharge oscillator physics where perturbations to SST in the eastern Pacific are either amplified or dampened through a series of feedbacks:

$$BJ = CD + TD + ZA + ED + TC$$

Here, CD is damping by the mean currents given by:

$$CD = -\left(\frac{\langle \bar{u} \rangle}{L_x} + \frac{\langle -2y\,\bar{v} \rangle}{{L_y}^2} + \frac{\langle H\left(\bar{w}\right)\bar{w} \rangle}{H_m} \right)$$

Angle brackets indicate the area average for the central-eastern Pacific (180–280ºE) and bars indicate a time-mean over the time length of the experiment. $\bar{u}$, $\bar{v}$ and $\bar{w}$are the mean zonal, meridional and vertical velocities in the mixed layer. L_x and L_y are the zonal and meridional scale lengths. H_m is the depth of the ocean mixed layer (50 m), and $H\left(\bar{w}\right)$ is the Heaviside step function, which ensures that only positive values of vertical velocity are taken into account.

TD is thermodynamic damping given by:

$$TD = -\alpha$$

Here, α is the linear regression coefficient from mixed layer temperature to net energy fluxE_{net}, from the ocean to the atmosphere. E_{net} is given by:

$$E_{net} = E_{incoming\_shortwave} + E_{incoming\_longewave} - E_{outgoing\_shortwave} - E_{outgoing\_longewave} - E_{latent\_heat} - E_{sensible\_heat}$$

α is further multiplied by $\frac{1}{\rho C_p H_m}$where ρ is sea water density and C_p is specific heat capacity of seawater and thus has units of $time^{-1}$.

ZA, EK and TC correspond to the zonal advection, Ekman and thermocline feedbacks respectively, given by:

$$ZA = \mu_a \beta_u \langle -\frac{\partial \bar{T}}{\partial x} \rangle \quad EK = \mu_a \beta_w \langle -\frac{\partial \bar{T}}{\partial z} \rangle \quad TC = \mu_a^* \beta_h \langle -\frac{\bar{w}}{H_m} \rangle$$

Where μ_a and $\mu_a^*$are linear regression coefficients between wind stress and SST anomalies. β_u, β_w, and β_h are the linear correlation coefficients between wind stress and zonal current, vertical current and thermocline anomalies respectively. $\frac{\partial \bar{T}}{\partial x}$ is the mean state zonal temperature gradient and $\frac{\partial \bar{T}}{\partial z}$ is the mean vertical stratification. $\bar{w}$ is the mean vertical velocity. All regression coefficients are for the central-east equatorial Pacific (180–280ºE), except μ_a^* which is calculated for the entire Pacific equatorial region (130–280ºE). Following Kim et al. (2014) and Ferrett and Collins (2019), we use temperature at 50 m depth as a proxy for thermocline anomalies. In a supplementary analysis, we then repeat Bjerknes Index calculation, but for the Niño3 region (210–280ºE) to illustrate how the relative role of damping and feedback terms change when a different range of averaging is used. The equatorial region is defined between 5ºS and 5ºN.

2.4 Noise

Finally, an important contribution to ENSO dynamics comes from atmospheric noise, which can drive a damped oscillation even when the BJ-index is negative. Here we define atmospheric noise in the tropics following Philip and Oldenborgh (2009) as:

$$\epsilon\left(x,y,t\right)=\tau_x\left(x,y,t\right)-\sum_{i=1}^{2}A_1\left(x,y\right)_i T^{'}{}_i\left(t\right)$$

Where $\epsilon\left(x,y,t\right)$denotes stochastic forcing by random wind stress variations,$T^{'}{}_i\left(t\right)$ is SST anomalies averaged over standard regions and$A_1\left(x,y\right)_i$ is the domain-wide wind stress patterns corresponding to the SST anomalies of the separate regions i = 1, 2. Here we use i = 1 as the Niño3 region, and i = 2 as the Niño4 region. We then average ϵ over the equatorial Pacific region (130–280ºE) and then take the standard deviation over time to estimate the noise magnitude.

3. Results

3.1 SST, rainfall and extreme event changes across multiple warming experiments

We find all models show an enhanced ENSO SST variability in the SSP5-8.5 scenario relative to the piControl experiment (in the ensemble-mean sense). Most models show a similar or slightly smaller increase of ENSO amplitude in the SSP1-2.6 scenario, yet the differences between the two scenarios are small compared to differences between the models. ENSO responses in the 1pctCO_2 scenario is also correlated to the SSP5-8.5 response, yet is more muted.

The abrupt-4xCO_2 scenario on average yields a poorer correlation with the SSP5-8.5 response and also has the largest spread among the experiments. In fact, 6 models in the 4xCO_2 scenario show a reduction in ENSO activity, with CESM2 having the most dramatic reduction (Fig. 1). By contrast, 2 models (ACCESS-ESM5-1 and FIO-2) show an increase that is larger than any ensemble member change in the SSP scenarios.

Changes in extreme El Niño events, defined through their Niño3 SST index, are expectedly linked to changes in ENSO SST amplitude, and there is a steep slope between ENSO amplitude and extreme events, such that a 25% increase in ENSO SST amplitude leads on average to an about 100% increase in the frequency of extreme El Niño events (Fig. 2). The strongest correlation between extreme events and ENSO SST is found in the abrupt-4xCO_2 experiments.

While the response of ENSO SST variability is highly dependent on both the experiment and model used, there is a universal increase in ENSO rainfall variability across all models and all experiments. In contrast to ENSO SST amplitude, the increase in ENSO precipitation variability is largest, on average, in the abrupt-4xCO_2 experiment (Fig. 3).

The next question is whether and how these ENSO changes are related to changes in the mean state of the tropical Pacific and other factors. We find that the correlation between changes in ENSO SST amplitude and in the mean state zonal SST gradient is weak (Fig. 4) and not statistically significant at the 99% level, while the correlation between changes in ENSO rainfall variability and in the mean zonal SST gradient is generally higher (Fig. 5a, 5b, 5c). Yet, the highest correlation is found between changes in variability of ENSO rainfall and SST (Fig. 5d, 5e, 5f). We also investigated whether changes in ENSO rainfall variability might be linked to the eastern equatorial Pacific warming, mean tropical warming and mean rainfall, but did not find any statistically significant correlations.

3.2 Changes to the Bjerknes Stability Index, thermodynamic damping and noise

To investigate the connection between mean state changes and ENSO SST response in a more quantitative manner, we compute the Bjerknes Stability Index (BJ Index) for a subset on models with available data. First, we compute this index using the central-eastern equatorial Pacific (180–280ºE) as the region of averaging following (Kim et al. 2014). This analysis reveals that all

models in the subset show an increase in mean state stability with warming. For 5 out of 7 models, an increase in thermodynamical damping α dominates the changes, driving a decrease in the Bjerknes Index, and hence increasing ENSO stability (Fig. 6). For two models (MIROC6 and MIROC-ES2L), the increase in α is more modest and a decrease in the thermocline feedback is a dominating term in the change of the Bjerknes Index with warming. For all models, the decrease in the Bjerknes Index is higher for abrupt-4xCO_2 than for SSP585, suggesting that a rapid strong increase in radiative forcing stabilizes the system in the linear stability sense. While changes to the damping terms are robust in response the warming, there is no consensus in changes to the feedback terms. The 5 out of 7 of models show an increase in the Ekman feedback, 4 out of 7 show an increase in the thermocline feedback while all models show only small changes in the zonal advection feedback.

We next recompute the Bjerknes Index but for the smaller Niño3 region (Supplementary Fig. 1). In this case, the computed Bjerknes Index is generally more negative, due to smaller positive feedback strengths compared with the full central-eastern Pacific region. For the global warming simulations, 5 out of 7 models show a more stable Niño3 Bjerknes Index, which is similar to the central-eastern Pacific Bjerknes Index. However, two models (MIROC6 and MIROC-ES2L) show a more unstable Bjerknes Index with warming for the Niño3 region, driven by an increase in the zonal advection and thermocline feedbacks. This could indicate that changes in the mean state of these two models lead to a more unstable Niño3 region, which might be able to explain a stronger ENSO SST in these two particular models. Even for these two models the use of the Bjerknes Index for explaining ENSO strengthening is problematic, given the strong sensitivity of the results to the choice of the averaging region.

Next, to examine potential changes in non-linearities that could counteract increased linear stability, we calculate changes to wind stress-SST coupling (μ_a) and thermodynamic damping (α) in three different ranges of temperature anomalies. We find that the thermodynamic damping α, while increasing in the central range of temperature anomalies (-1 ^{o}C to 1 ^{o}C), decreases in the CanESM5, CESM2, CNRM-CM6-1, HadGEM3-CG31-LL for SST anomalies above 1 ^{o}C (Supplementary Fig. 2). This suggests that changes in α, which dominate the Bjerknes Index, may be overestimated in some models because the damping becomes less efficient for larger temperature anomalies for some models. The coupling coefficient μ_a becomes stronger with warming in the majority of models in the central SST anomaly range (-1 ^{o}C to 1 ^{o}C), while for the IPSL-CM6A-LR, MIROC6 and MIROC-ES2L, μ_a reduces for temperature anomalies below − 1 ^{o}C in warming experiments (Supplementary Fig. 3). One however has to be careful in interpreting this result as the correlations may become very small for the high and low SST ranges.

To further investigate the discrepancy between changes in the Bjerknes Index and ENSO response, we also analyze changes to atmospheric noise among the models for which wind stress data was available. Atmospheric noise, including westerly wind bursts that occur frequently in the tropical Pacific, is believed to play an important role in sustaining ENSO and especially extreme El Niño events (Puy et al. 2019; Yu and Fedorov 2020; Fedorov 2002). We find that on average, the correlation between change in atmospheric noise and change in ENSO (Fig. 7) is significant and higher than between change in mean state and ENSO SST amplitude, indicating that atmospheric noise could play an important role in ENSO changes with warming, despite some outliers in the abrupt-4xCO_2 experiment, and potentially explain the general strengthening of ENSO with warming. However, quantifying this relationship is difficult because (1) the computations of the Bjerknes index and noise amplitude is sensitive to the choice of the averaging regions and (2) the question of causality is difficult to resolve as the noise can increase as a result of strengthening of ENSO.

3.3 Long-term warming experiments

Lastly, we investigate three 1000-year simulations for the abrupt-4xCO_2 experiment for three models (ACCESS-ESM1-5, CESM2 and IPSL-CM6A-LR). We find that even after such a long time ENSO response does not converge in these models. Specifically, CESM2 shows a drastic reduction in ENSO strength, such that at the end of the simulation its amplitude reaches only about 1/3 of that in the control. In ACCESS-ESM1-5 ENSO remains stronger than the control throughout the simulation period (Fig. 8), while in IPSL-CM6A-LR ENSO does not change much over the first 600 years, but then strengthens.

Discussion and conclusions

We have investigated the ENSO response to warming in four different scenarios with realistic and idealized radiative forcing across 20 models. We found that most of the models show enhanced ENSO SST variability in all warming scenarios considered. Moreover, in a high-forcing scenario SSP5-8.5, each model shows a stronger ensemble mean ENSO. Yet, there are large inter-

model differences, which play a greater role than scenario uncertainty. The majority of models do show a generally consistent response across different types of warming experiments indicating that the observed response is indeed a result of radiative forcing, and the spread among models is primarily caused by factors other than natural variability.

Interestingly, for the majority of models, gradual CO_2-increase SSP scenarios on average show a stronger ENSO response to warming than the abrupt-4xCO2 scenario. In fact, roughly 40% of the models considered show a weakening or no change of ENSO SST variability in this scenario, which implies that caution should be taken when relying on such experiments for making projections of ENSO future changes.

Despite this uncertainty in ENSO SST response, ENSO rainfall variability in the tropics increases universally across all experiments and models, which has important consequences for adaptation and mitigation as changes to floods and droughts may cause more damage than changes to SST itself and as ENSO remote teleconnections depend of latent heat release. The fact that rainfall variability increases robustly with warming is expected given that a warmer atmosphere can hold more water following the Clausius-Clapeyron relation and eastern Pacific warming can reduce the convection barrier for El Niño events (Yun et al. 2021). However, we find that changes in the background state alone cannot fully account for the modeled change in ENSO rainfall variability as changes in SST variability play a critical role as well. This highlights the need to better understand the response of ENSO SST variability in order to improve predictions for ENSO rainfall response.

Extreme events can change drastically given a small change in ENSO SST amplitude and models with a relatively modest change in ENSO SST variability may show up to a doubling of the number of extreme El Niño events. This close connection between extreme events and ENSO SST amplitude is evident even in a relatively short timeframe of 150 years. The fact that the change in ENSO SST variability is closely connected to an increase in extreme events, which, like increases in ENSO rainfall, has important consequences for adaptation and mitigation as extreme events are often associated with more damage for society than a change in mean conditions (Trenberth 2012). Given the sensitivity of extreme events to small changes in ENSO SST, it is crucial to improve projections of ENSO SST amplitude with warming across models and warming experiments.

In attempt to explain the robust strengthening of ENSO in warming scenarios we compute changes in the Bjerknes Stability Index but find it to be a poor predictor for changes in ENSO in a small subset of models (7), which is similar to findings in other studies using the Bjerknes Index for individual models (Manucharyan and Fedorov 2014; Ferrett and Collins 2019). Like Callahan et al. (2021), we find the increased thermodynamic damping to be the most important term in the Bjerknes Index for 5 out of 7 models, yielding a more stable Bjerknes index those models. However, the fact that all models show a stronger ENSO SST variability in the SSP585 scenario points to other effects counteracting this stability increase. For example, here we show that the thermodynamic damping may be overestimated in the models due to a nonlinear relationship between SST and surface energy fluxes. We show that the coupling between SST and surface heat fluxes decrease in warming experiments above a threshold of 1^o C SST anomalies in 4 out of 7 models, which could explain why ENSO SST amplitude can increase despite a stronger thermodynamic damping in a linear sense.

MIROC6 and MIROC-ES2L show a decrease in the Bjerknes Stability Index for the Niño3 region as opposed to other models for which the Bjerknes Index is calculated. These models, together with EC-Earth3 and EC-Earth3-Veg, are outliers among the 20 models analyzed in that they show a drastic increase in ENSO amplitude across experiments. Thus, a decrease in stability for the Niño3 region, driven by increases in feedbacks in the eastern Pacific, may explain why some models have a drastic increase in ENSO amplitude, but it cannot explain the robust increase in ENSO across models.

We suggest here that atmospheric noise, including westerly wind bursts, may play a crucial role in driving changes to ENSO, which is supported by a strong correlation between changes to noise and ENSO SST variability as well as other studies (C. Wengel et al. 2018; Lopez et al. 2022), but questions remain whether this noise is in fact driving a stronger ENSO, as ENSO itself can also generate more noise (Kug et al. 2008; Eisenman, Yu, and Tziperman 2005).

This result highlights a problematic gap in our understanding on what drives changes in ENSO in response to CO_2 in GCMs, as we cannot understand changes in ENSO in terms of a simple linear Bjerknes stability framework that links those changes to changes in the tropical mean state. This is exemplified by the fact that mean state changes are larger for the abrupt-4xCO_2

scenario, and yet by century-end ENSO amplitude increases more in the SSP585 scenario. In fact, 5 or 6 models in this scenario actually show a weaker ENSO. It is feasible that more comprehensive linear stability analyses, computing the full leading eigen modes of the system (e.g. Sévellec and Fedorov 2013 or Fedorov and Philander 2001) could provide more consistent results, but this is yet to be done for coupled GCMs.

Overall, our results point towards a robust increase in ENSO activity in the SSP5-8.5 and SSP1-2.6 scenarios, yet a common mechanism to explain these changes is lacking. Models that show a drastic increase in ENSO amplitude, such as the MIROC6 and MIROC-ES2L models may be driven by stability changes over the Nino3 region in combination with a small change or no change in thermodynamic damping. On the contrary, for models with a moderate change in ENSO, the linear Bjerknes Index decreases – primarily because of increased thermodynamic damping, leading to a more stable system. This suggests that atmospheric noise and/or nonlinear changes may drive a stronger ENSO for these models. On the other hand, for CESM2, which showed a weaker ENSO with $4xCO_2$, the Bjerknes Index did show the largest reduction, driven by increased thermodynamic damping and a decrease in the thermocline feedback. Yet, the same model shows an increase in ENSO, albeit small, for SSP5-8.5 and SSP1-2.6 relative to piControl.

ENSO amplitude on average also increases for high CO_2 scenarios, such as the $1pctCO_2$ or abrupt-$4xCO_2$ scenario, although the change is less robust across models. Furthermore, in contrast to Wenger et al. (2021) we did not find evidence that models converge to a weaker ENSO in the abrupt $4xCO_2$ experiments over longer time-scales. In fact, ENSO remains stronger than the control in several models considered even after 1000 years of computation. On the whole, the abrupt $4xCO_2$ scenario produces the broadest spread of ENSO projections, and as such may not be the most reliable indicator of changes to come. These findings highlight that despite the robust strengthening of ENSO by century-end in a broad range of models and warming scenarios of CMIP6, there is still a large uncertainty in ENSO future response to global warming, which should be addressed by evaluating ENSO drivers across multiple warming experiments in multiple models.

Declarations

Funding

U.K.H. is supported by a NASA FINESST Fellowship (80NSSC20K1634). A.V.F. is supported by grants from NASA (80NSSC21K0558) and NOAA (NA20OAR4310377). Additional funding is provided by the ARCHANGE project (ANR-18-MPGA-0001, France). We also acknowledge a generous gift to Yale University from T. Sandoz. The funders had no role in study design, data collection and analysis, decision to publish or preparation of the manuscript

Competing interests

The authors declare no competing interests.

Data Availability

CMIP6 data are available at https://esgf-node.llnl.gov/search/cmip6/. Code used for the analysis is available per request and at Gibhub upon publication.

Author contributions

U.K.H. and A.V.F. contributed equally to designing the research. U.K.H. performed the data analysis and, together with A.V.F., interpreted the results. U.K.H. wrote the manuscript and edited it together with A.V.F.

References

1. Brown, Josephine R., Chris M. Brierley, Soon-Il An, Maria-Vittoria Guarino, Samantha Stevenson, Charles J. R. Williams, Qiong Zhang, et al. 2020. ‘Comparison of Past and Future Simulations of ENSO in CMIP5/PMIP3 and CMIP6/PMIP4 Models’. Preprint. Climate Modelling/Modelling only/Pleistocene. https://doi.org/10.5194/cp-2019-155.

2. Cai, Wenju, Benjamin Ng, Guojian Wang, Agus Santoso, Lixin Wu, and Kai Yang. 2022. 'Increased ENSO Sea Surface Temperature Variability under Four IPCC Emission Scenarios'. *Nature Climate Change* 12 (3): 228–31. https://doi.org/10.1038/s41558-022-01282-z.
3. Cai, Wenju, Agus Santoso, Matthew Collins, Boris Dewitte, Christina Karamperidou, Jong-Seong Kug, Matthieu Lengaigne, et al. 2021. 'Changing El Niño–Southern Oscillation in a Warming Climate'. *Nature Reviews Earth & Environment* 2 (9): 628–44. https://doi.org/10.1038/s43017-021-00199-z.
4. Cai, Wenju, Agus Santoso, Guojian Wang, Sang-Wook Yeh, Soon-Il An, Kim M. Cobb, Mat Collins, Eric Guilyardi, Fei-Fei Jin, and Jong-Seong Kug. 2015. 'ENSO and Greenhouse Warming'. *Nature Climate Change* 5 (9): 849–59.
5. Cai, Wenju, Guojian Wang, Boris Dewitte, Lixin Wu, Agus Santoso, Ken Takahashi, Yun Yang, Aude Carréric, and Michael J. McPhaden. 2018. 'Increased Variability of Eastern Pacific El Niño under Greenhouse Warming'. *Nature* 564 (7735): 201–6. https://doi.org/10.1038/s41586-018-0776-9.
6. Callahan, Christopher W., Chen Chen, Maria Rugenstein, Jonah Bloch-Johnson, Shuting Yang, and Elisabeth J. Moyer. 2021. 'Robust Decrease in El Niño/Southern Oscillation Amplitude under Long-Term Warming'. *Nature Climate Change* 11 (9): 752–57. https://doi.org/10.1038/s41558-021-01099-2.
7. DiNezio, Pedro N., Ben P. Kirtman, Amy C. Clement, Sang-Ki Lee, Gabriel A. Vecchi, and Andrew Wittenberg. 2012. 'Mean Climate Controls on the Simulated Response of ENSO to Increasing Greenhouse Gases'. *Journal of Climate* 25 (21): 7399–7420.
8. Eisenman, Ian, Lisan Yu, and Eli Tziperman. 2005. 'Westerly Wind Bursts: ENSO's Tail Rather than the Dog?' *Journal of Climate* 18 (24): 5224–38.
9. Fedorov, Alexey V. 2002. 'The Response of the Coupled Tropical Ocean–Atmosphere to Westerly Wind Bursts'. *Quarterly Journal of the Royal Meteorological Society* 128 (579): 1–23. https://doi.org/10.1002/qj.200212857901.
10. Fedorov, Alexey V., and S. George Philander. 2000. 'Is El Niño Changing?' *Science* 288 (5473): 1997–2002.
11. ———. 2001. 'A Stability Analysis of Tropical Ocean–Atmosphere Interactions: Bridging Measurements and Theory for El Niño'. *Journal of Climate* 14 (14): 3086–3101. https://doi.org/10.1175/1520-0442(2001)014<3086:ASAOTO>2.0.CO;2.
12. Ferrett, Samantha, and Matthew Collins. 2019. 'ENSO Feedbacks and Their Relationships with the Mean State in a Flux Adjusted Ensemble'. *Climate Dynamics* 52 (12): 7189–7208. https://doi.org/10.1007/s00382-016-3270-9.
13. Fredriksen, Hege-Beate, Judith Berner, Aneesh C. Subramanian, and Antonietta Capotondi. 2020. 'How Does El Niño–Southern Oscillation Change Under Global Warming—A First Look at CMIP6'. *Geophysical Research Letters* 47 (22): e2020GL090640. https://doi.org/10.1029/2020GL090640.
14. Heede, Ulla, and Alexey Fedorov. 2021. 'Eastern Equatorial Pacific Warming Delayed by Aerosols and Thermostat Response to CO2'.
15. Heede, Ulla K., Alexey V. Fedorov, and Natalie J. Burls. 2020. 'Timescales and Mechanisms for the Tropical Pacific Response to Global Warming: A Tug of War between the Ocean Thermostat and Weaker Walker'. *Journal of Climate*, April. https://doi.org/10.1175/JCLI-D-19-0690.1.
16. ———. 2021. 'A Stronger versus Weaker Walker: Understanding Model Differences in Fast and Slow Tropical Pacific Responses to Global Warming'. *Climate Dynamics*, 1–18.
17. Huang, Ping, and Shang-Ping Xie. 2015. 'Mechanisms of Change in ENSO-Induced Tropical Pacific Rainfall Variability in a Warming Climate'. *Nature Geoscience* 8 (12): 922–26. https://doi.org/10.1038/ngeo2571.
18. Jin, Fei-Fei, Seon Tae Kim, and Luis Bejarano. 2006. 'A Coupled-Stability Index for ENSO'. *Geophysical Research Letters* 33 (23). https://doi.org/10.1029/2006GL027221.
19. Kim, Seon Tae, Wenju Cai, Fei-Fei Jin, and Jin-Yi Yu. 2014. 'ENSO Stability in Coupled Climate Models and Its Association with Mean State'. *Climate Dynamics* 42 (11): 3313–21.
20. Kohyama, Tsubasa, Dennis L. Hartmann, and David S. Battisti. 2018. 'Weakening of Nonlinear ENSO Under Global Warming'. *Geophysical Research Letters* 45 (16): 8557–67. https://doi.org/10.1029/2018GL079085.
21. Kug, Jong-Seong, Fei-Fei Jin, K. P. Sooraj, and In-Sik Kang. 2008. 'State-Dependent Atmospheric Noise Associated with ENSO'. *Geophysical Research Letters* 35 (5). https://doi.org/10.1029/2007GL032017.

22. Lopez, Hosmay, Sang-Ki Lee, Dongmin Kim, Andrew T. Wittenberg, and Sang-Wook Yeh. 2022. 'Projections of Faster Onset and Slower Decay of El Niño in the 21st Century'. *Nature Communications* 13 (1): 1915. https://doi.org/10.1038/s41467-022-29519-7.
23. Manucharyan, Georgy E., and Alexey V. Fedorov. 2014. 'Robust ENSO across a Wide Range of Climates'. *Journal of Climate* 27 (15): 5836–50. https://doi.org/10.1175/JCLI-D-13-00759.1.
24. McPhaden, Michael J., Agus Santoso, and Wenju Cai. 2020. *El Niño Southern Oscillation in a Changing Climate*. Vol. 253. John Wiley & Sons.
25. O'Neill, Brian C., Claudia Tebaldi, Detlef P. van Vuuren, Veronika Eyring, Pierre Friedlingstein, George Hurtt, Reto Knutti, et al. 2016. 'The Scenario Model Intercomparison Project (ScenarioMIP) for CMIP6'. *Geoscientific Model Development* 9 (9): 3461–82. https://doi.org/10.5194/gmd-9-3461-2016.
26. Philip, Sjoukje, and Geert Jan van Oldenborgh. 2009. 'Significant Atmospheric Nonlinearities in the ENSO Cycle'. *Journal of Climate* 22 (14): 4014–28. https://doi.org/10.1175/2009JCLI2716.1.
27. Puy, Martin, Jérôme Vialard, Matthieu Lengaigne, Eric Guilyardi, Pedro N. DiNezio, Aurore Voldoire, Magdalena Balmaseda, Gurvan Madec, Christophe Menkes, and Michael J. Mcphaden. 2019. 'Influence of Westerly Wind Events Stochasticity on El Niño Amplitude: The Case of 2014 vs. 2015'. *Climate Dynamics* 52 (12): 7435–54. https://doi.org/10.1007/s00382-017-3938-9.
28. Ropelewski, C. F., and M. S. Halpert. 1987. 'Global and Regional Scale Precipitation Patterns Associated with the El Niño/Southern Oscillation'. *Monthly Weather Review* 115 (8): 1606–26. https://doi.org/10.1175/1520-0493(1987)115<1606:GARSPP>2.0.CO;2.
29. Sévellec, Florian, and Alexey V. Fedorov. 2013. 'The Leading, Interdecadal Eigenmode of the Atlantic Meridional Overturning Circulation in a Realistic Ocean Model'. *Journal of Climate* 26 (7): 2160–83. https://doi.org/10.1175/JCLI-D-11-00023.1.
30. Trenberth, Kevin E. 2012. 'Framing the Way to Relate Climate Extremes to Climate Change'. *Climatic Change* 115 (2): 283–90. https://doi.org/10.1007/s10584-012-0441-5.
31. Vecchi, Gabriel A., Brian J. Soden, Andrew T. Wittenberg, Isaac M. Held, Ants Leetmaa, and Matthew J. Harrison. 2006. 'Weakening of Tropical Pacific Atmospheric Circulation Due to Anthropogenic Forcing'. *Nature* 441 (7089): 73–76.
32. Wengel, C., D. Dommenget, M. Latif, T. Bayr, and A. Vijayeta. 2018. 'What Controls ENSO-Amplitude Diversity in Climate Models?' *Geophysical Research Letters* 45 (4): 1989–96. https://doi.org/10.1002/2017GL076849.
33. Wengel, Christian, Sun-Seon Lee, Malte F. Stuecker, Axel Timmermann, Jung-Eun Chu, and Fabian Schloesser. 2021. 'Future High-Resolution El Niño/Southern Oscillation Dynamics'. *Nature Climate Change* 11 (9): 758–65. https://doi.org/10.1038/s41558-021-01132-4.
34. Yeh, Sang-Wook, Wenju Cai, Seung-Ki Min, Michael J. McPhaden, Dietmar Dommenget, Boris Dewitte, Matthew Collins, et al. 2018. 'ENSO Atmospheric Teleconnections and Their Response to Greenhouse Gas Forcing'. *Reviews of Geophysics* 56 (1): 185–206. https://doi.org/10.1002/2017RG000568.
35. Yu, Sungduk, and Alexey V. Fedorov. 2020. 'The Role of Westerly Wind Bursts During Different Seasons Versus Ocean Heat Recharge in the Development of Extreme El Niño in Climate Models'. *Geophysical Research Letters* 47 (16): e2020GL088381. https://doi.org/10.1029/2020GL088381.
36. Yun, Kyung-Sook, June-Yi Lee, Axel Timmermann, Karl Stein, Malte F. Stuecker, John C. Fyfe, and Eui-Seok Chung. 2021. 'Increasing ENSO–Rainfall Variability Due to Changes in Future Tropical Temperature–Rainfall Relationship'. *Communications Earth & Environment* 2 (1): 1–7. https://doi.org/10.1038/s43247-021-00108-8.

Figures

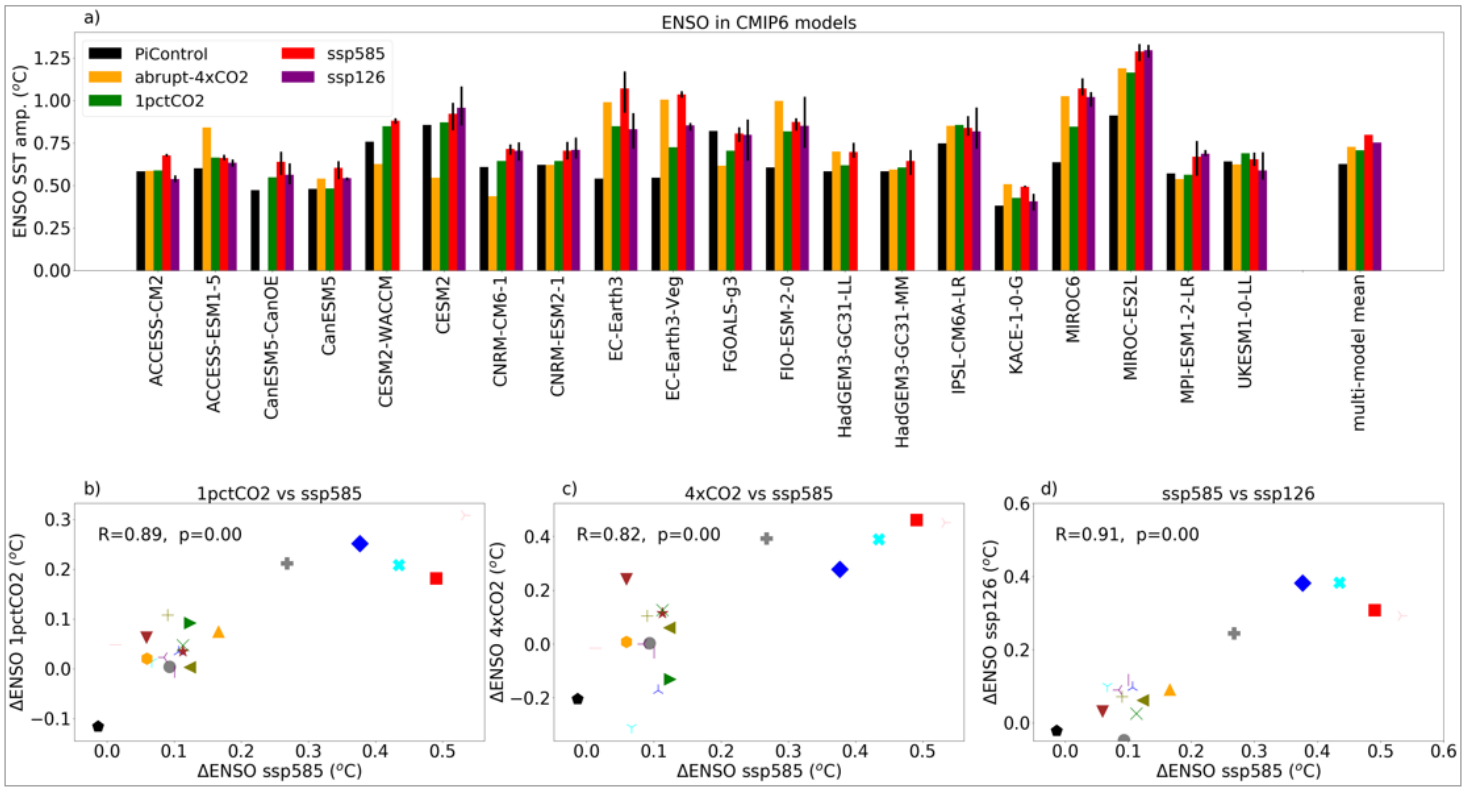

Figure 1

Overview of ENSO changes in CMIP6 models across different experiments. *(a) A barplot showing the time-mean amplitude of ENSO SST variability (Methods) in individual models for the piControl, abrupt-4xCO2, 1pctCO2, SSP585 and SSP126 experiments, respectively. Thin errorbars for SSP experiments indicate the maximum and minimum values across three ensemble members. (b), (c) and (d) Changes in ENSO SST amplitude in the 1pctCO2, abrupt4xCO2 and SSP126 scenarios, respectively, versus the SSP585 scenario. These changes are calculated relative to the piControl time-mean ENSO SST amplitude. Each marker+color combination signifies the same model across all plots as given by Table 1. The corresponding correlations and p-values are shown at the top left corners of the bottom panels. The high correlations suggest a general consistency of ENSO response across different types of warming experiments.*

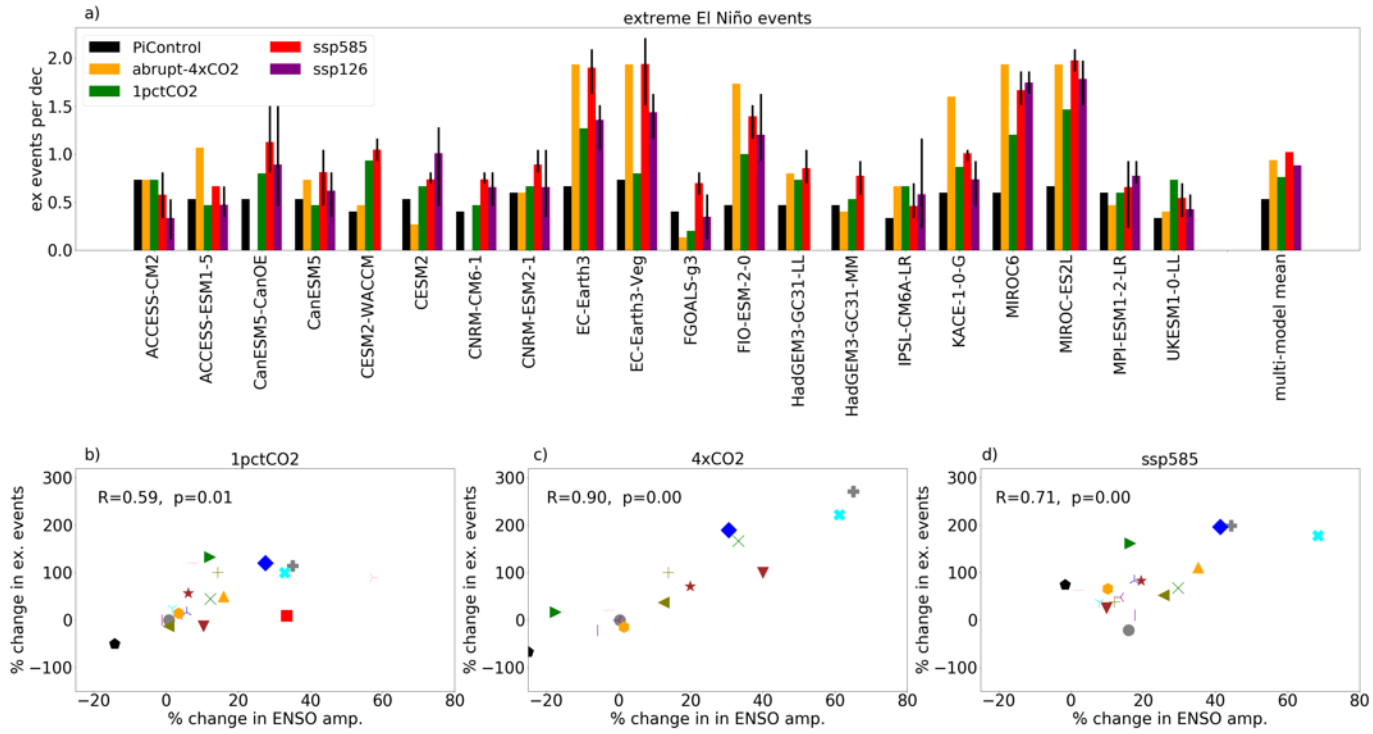

Figure 2

Overview of changes in extreme El Nino events. *(a) A barplot showing the time-mean frequency of extreme ENSO SST events (Methods) for the piControl, abrupt-4xCO2, 1pctCO2, SSP585 and SSP126 experiments, respectively. Thin errorbars for SSP-experiments indicate the maximum and minimum values across three ensemble members. (b), (c) and (d) Relative changes (%) in the frequency of extreme events versus changes in ENSO SST amplitude in the 1pctCO2, abrupt4xCO2 and SSP585 scenarios, respectively. Note that changes are calculated relative to the piControl time-mean ENSO SST variability. Each marker+color combination signifies the same model across all plots as given in Table 1. Note the robust increase in the frequency of extreme El Nino event in most models.*

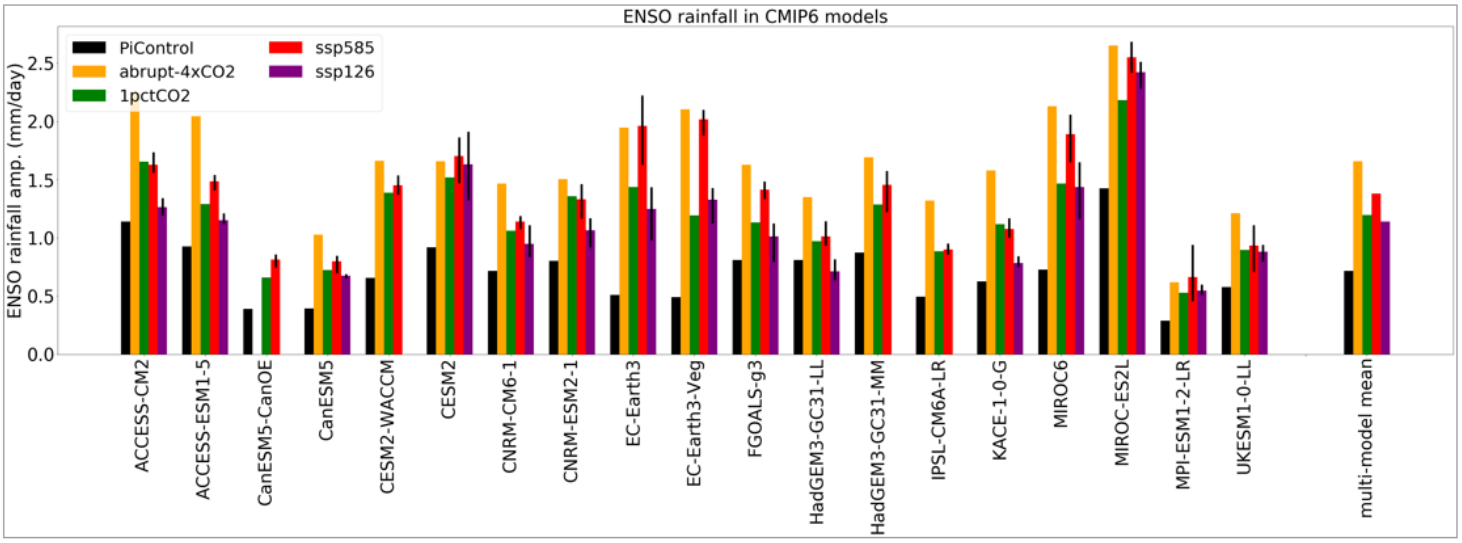

Figure 3

Overview of ENSO precipitation changes. *A barplot showing the time-mean individual model ENSO rainfall variability (see methods) for the piControl, abrupt-4xCO2, 1pctCO2, SSP585 and SSP126 experiments respectively. Thin errorbars for SSP-experiments indicate the maximum and minimum values across three ensemble members.*

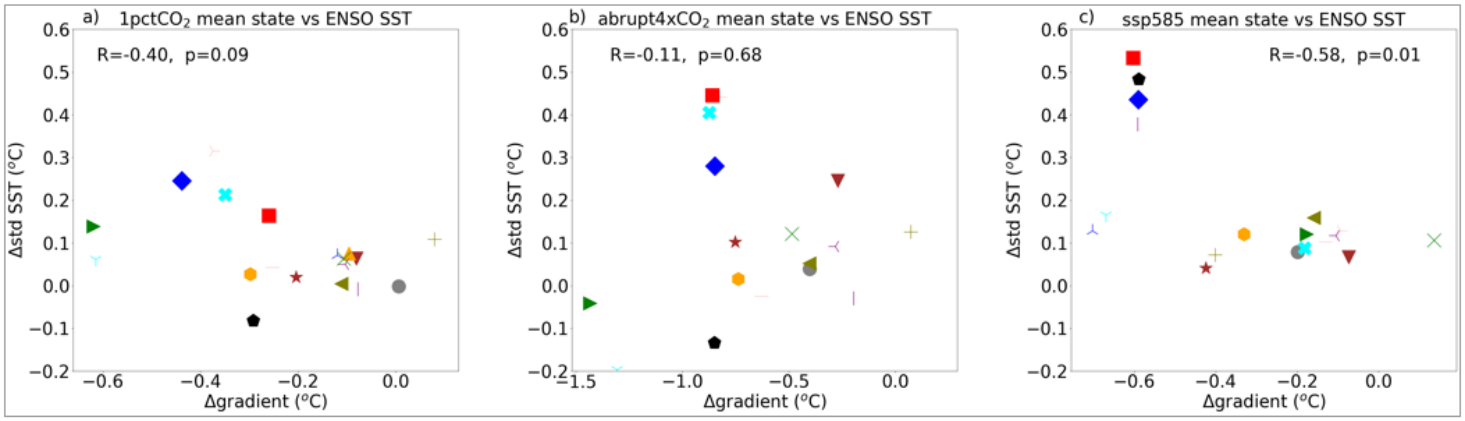

Figure 4

Linking ENSO SST variability changes to changes in the mean state east-west SST gradient. *(a), (b), (c) Changes in ENSO SST variability amplitude versus changes in the zonal SST mean gradient for the 1pctCO2, abrupt-4xCO2 and SSP585 scenarios. Each marker+color combination signifies the same model across all plots as given by Table 1. The corresponding correlations and p-values are shown at the top of each panel. Negative values on the horizontal axes indicate the SST gradient weakening. Across the models, the link between ENSO SST variability and the mean zonal gradient appears to be weak, even though there is a general tendency towards stronger ENSO when this gradient relaxes in the 1pctCO2 and SSP585 scenarios.*

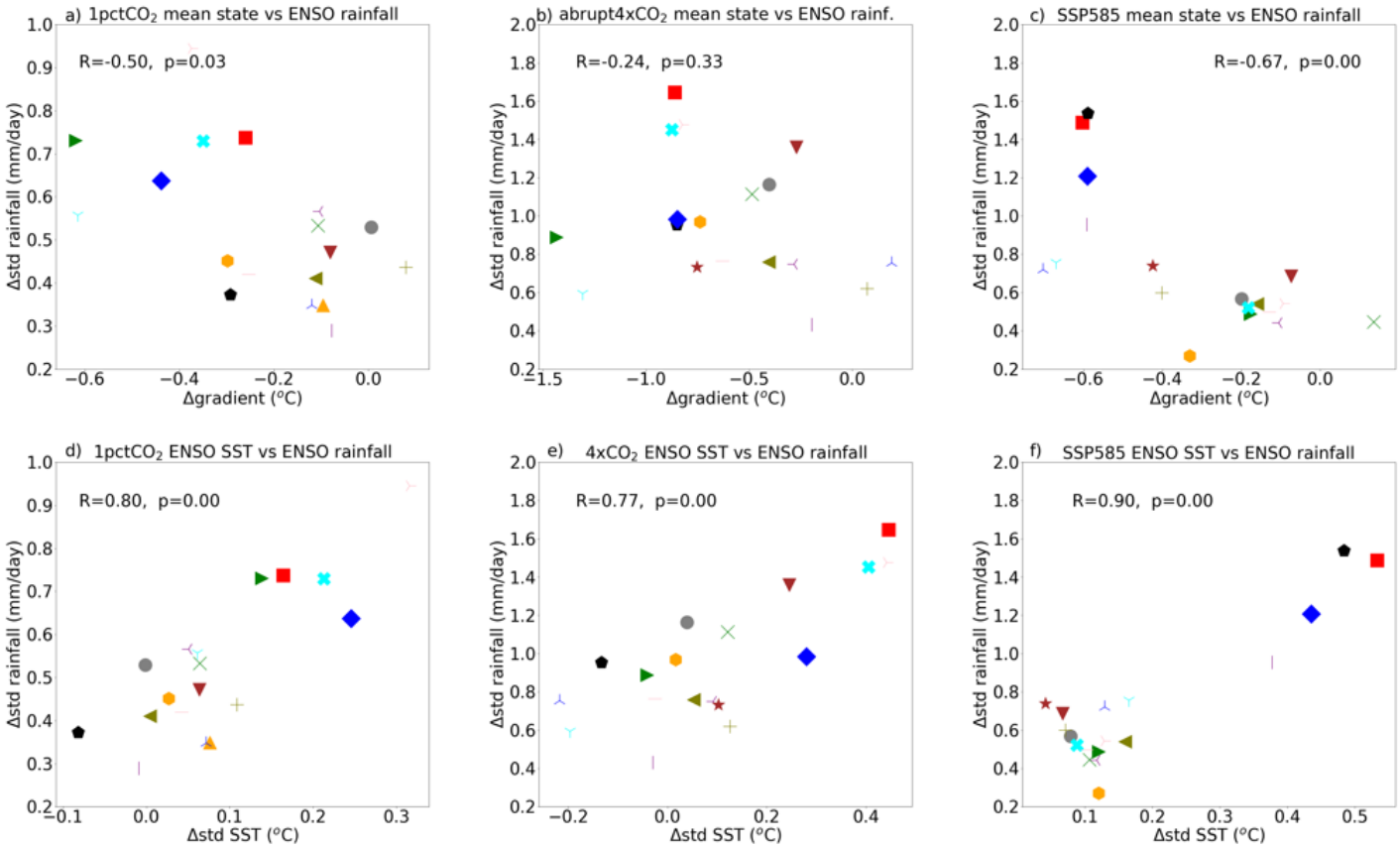

Figure 5

Linking ENSO rainfall variability changes to changes in SST mean state gradient and variability. *(a), (b), (c) Changes in ENSO rainfall variability versus changes in the zonal SST mean gradient for the 1pctCO2, abrupt-4xCO2 and SSP585 scenarios. (d), (e), (f) The same but versus changes in ENSO SST variability amplitude. Each marker+color combination signifies the same model across all plots as given by Table 1. The corresponding correlations and p-values are shown at the top of each panel.*

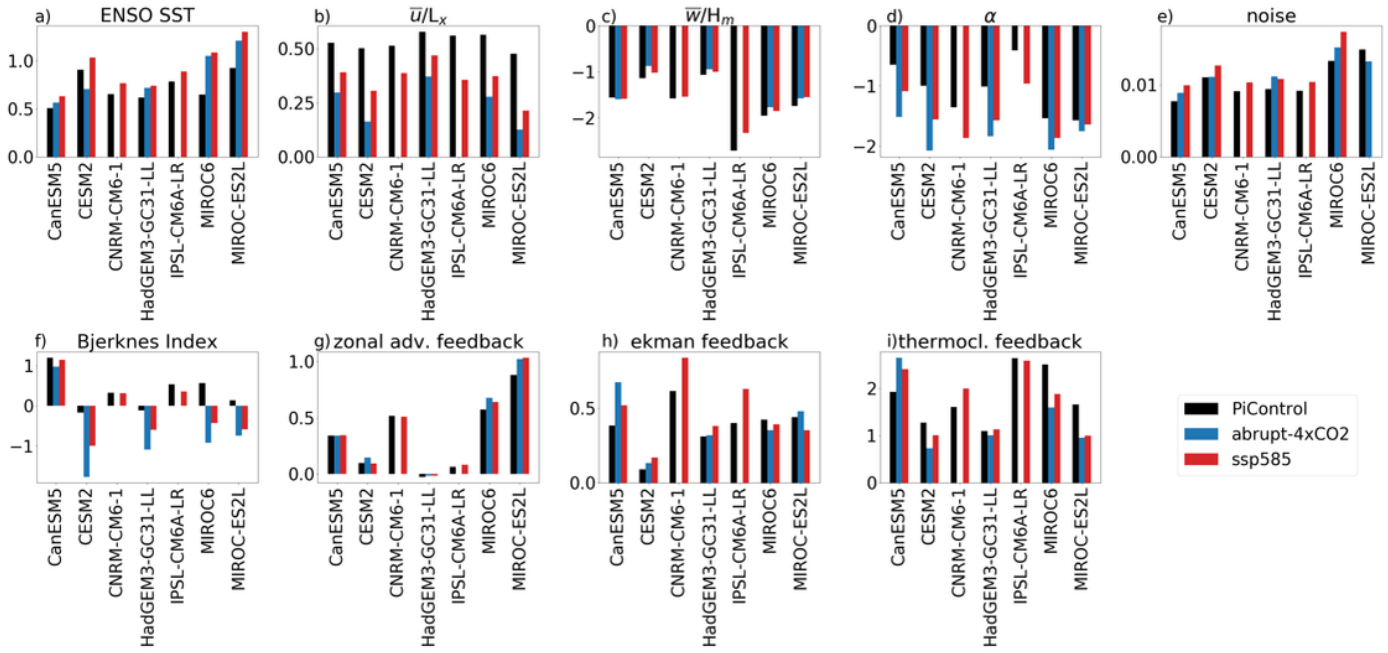

Figure 6

The Bjerknes stability Index and its contributing terms for a subset of models. *Panel (a) shows the changes in ENSO SST amplitude for a subset of models for the piControl, abrupt-4xCO2 and the SSP585 experiments. (b),(c),(d) show each of the major damping terms in the Bjerknes Index, and (e), (f) (g) show the three positive feedback terms for those same experiments. (h) shows the noise and (i) shows the overall Bjerknes Index value. All Bjerknes values are in units of year^{-1}. Noise is in the units of N m^{-2} and ENSO SST is in the units of ^{o}C. The Bjerknes index is computed for the region 180^{o}-280^{o} E (c.f. Supplementary Fig. 1 using the Niño3 region).*

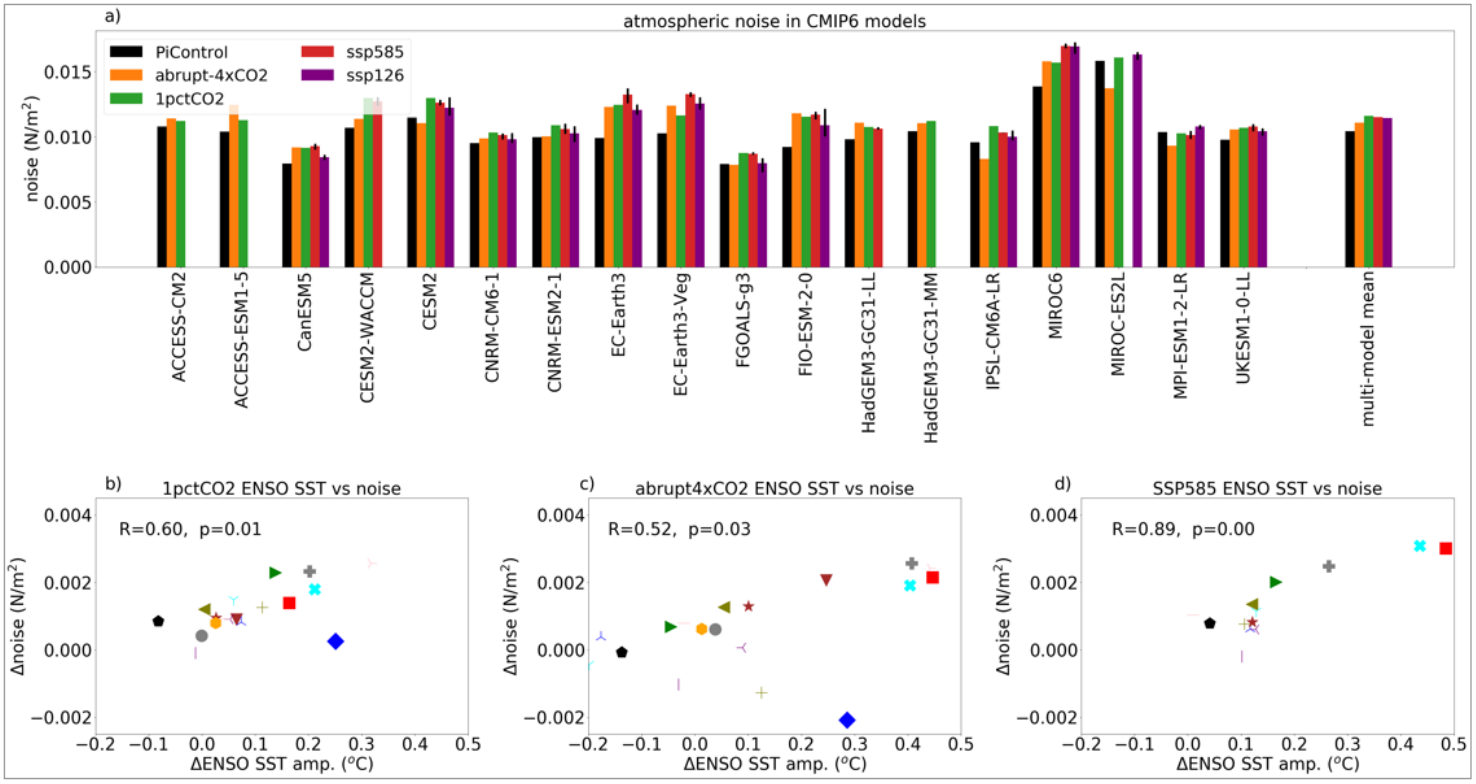

Figure 7

Overview of changes atmospheric noise in the tropical Pacific. *(a) A barplot showing the time-mean amplitude of model atmospheric noise (Methods) for the piControl, abrupt-4xCO_2, 1pctCO_2, and SSP585 experiments, respectively. Thin errorbars for SSP-experiments indicate the maximum and minimum values across three ensemble members. (b), (c) and (d) shows changes in noise amplitude versus changes in ENSO SST amplitude in the abrupt-4xCO2, 1pctCO2, and SSP585 experiments, respectively. The corresponding correlations and p-values are shown at the top of each panel.*

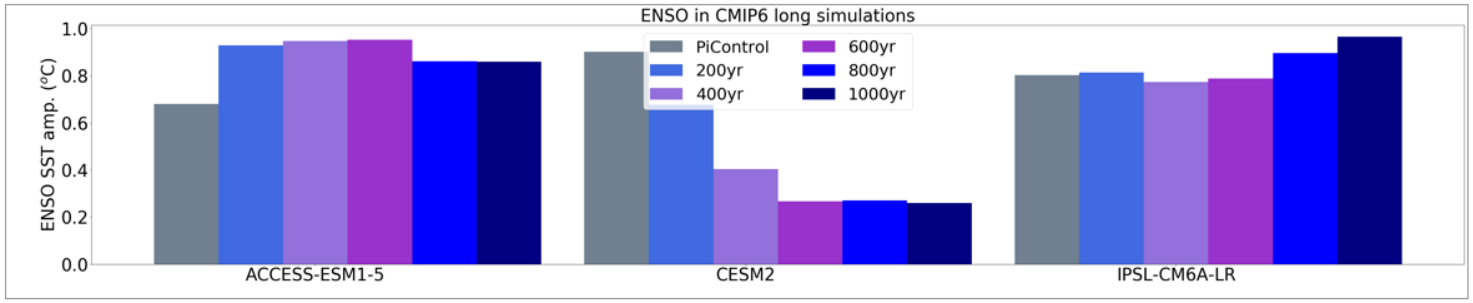

Figure 8

Simulated long-term changes in ENSO. *The plot shows ENSO SST amplitude estimated for consecutive 200-year time intervals of 1000-year abrupt-4xCO_2 simulations using three different climate models.*

Supplementary Files

This is a list of supplementary files associated with this preprint. Click to download.

- Supplementary.docx